Article

Image Processing and Measurement of the Bubble Properties in a Bubbling Fluidized Bed Reactor

Rajan Jaiswal [1,*]**, Britt. M. E. Moldestad** [1]**, Marianne S. Eikeland** [1]**, Henrik K. Nielsen** [2]
and Rajan Kumar Thapa [1]

[1] Department of Process, Energy and Environmental Technology, Faculty of Technology, Natural Sciences and Maritime Sciences, Campus Porsgrunn, University of South-Eastern Norway, Kjølnes 56, 3918 Porsgrunn, Norway

[2] Department of engineering sciences, Faculty of engineering and science, University of Agder, Jon Lilletuns vei 9, 4879 Grimstad, Norway

*   Correspondence: rajan.jaiswal@usn.no; Tel.: +47-48666290

Abstract: The efficiency of a fluidized bed reactor depends on the bed fluid dynamic behavior, which is significantly influenced by the bubble properties. This work investigates the bubble properties of a bubbling fluidized bed reactor using computational particle fluid dynamic (CPFD) simulations and electrical capacitance tomography (ECT) measurements. The two-dimensional images (along the reactor horizontal and vertical planes) of the fluidized bed are obtained from the CPFD simulations at different operating conditions. The CPFD model was developed in a commercial CPFD software Barracuda Virtual Reactor 20.0.1. The bubble behavior and bed fluidization behavior are characterized form the bubble properties: average bubble diameter, bubble rise velocity, and bubble frequency. The bubble properties were determined by processing the extracted images with script developed in MATLAB. The CPFD simulation results are compared with experimental data (obtained from the ECT sensors) and correlations in the literature. The results from the CPFD model and experimental measurement depicted that the average bubble diameter increased with an increase in superficial gas velocities up to 4.2 U_{mf} and decreased with a further increase in gas velocities due to the onset of large bubbles (potential slugging regime). The bubble rise velocity increased as it moved from the lower region to the bed surface. The Fourier transform of the transient solid volume fraction illustrated that multiple bubbles pass the plane with varying amplitude and frequency in the range of 1–6 Hz. Further, the bubble frequency increased with an increase in superficial gas velocity up to $2.5U_{mf}$ and decreased with a further increase in gas velocity. The CPFD model and method employed in this work can be useful for studying the influence of bubble properties on conversion efficiency of a gasification reactor operating at high temperatures.

Keywords: fluidized bed; bubble diameter; bubble rise velocity; bubble frequency; computational particle fluid dynamic; image processing

1. Introduction

Fluidized beds are extensively used in applications such as chemical regeneration, catalytic conversion, gasification, chemical synthesis, and pneumatic transportation, and each of these process applications requires a unique fluidization regime. The fluidization bed regimes include minimum fluidization, bubbling, turbulent, fast fluidization, and pneumatic conveying [1–4]. The types of regimes are mainly dependent on the fluidizing gas velocity, density, and particles size of the bed material, aspect ratio, and reactor dimension [5,6]. The major advantages of fluidized bed include efficient heat transfer, better temperature control, good mixing, and better solid circulation. In order to achieve the benefits of a fluidized bed, firstly, the reactor must be operated strictly within the specific fluidization regime required for the process. Secondly, the problem associated with

fluidized beds must be avoided for a smooth reactor operation and to achieve the desired process efficiency. However, the two-phase flow of gas–solid coupled with heat and mass transfer and series reactions in the fluidized bed reactors are complex and not yet fully understood. Challenges in operating fluidized bed reactors such as lower chemical conversion, non-uniform products, agglomeration, entrainment of particles, and reactor failure are often reported. These difficulties encountered while operating fluidized bed reactors can be overcome with a thorough understanding of the fluid dynamic behavior of the reactor and bubble dynamics in the bed. The major objective of this paper is to investigate the fluid dynamics behavior of a bubbling fluidized bed (BFB) which is significantly influenced by the bubble properties.

An appropriate regime in a bubbling fluidized bed can be characterized by the better fluidization quality of the bed without any slug. Ideally, for better fluidizing quality of the bubbling bed, the bubbles should be large in number, uniformly distributed across the bed, and smaller in size. The bubbles formed in a fluidized bed are primarily responsible for good solid circulation, and gas–solid contact area, which determines the heat and mass transfer within the reactor. As the bubble rises from the bottom of the bed to the top, it carries particles with it, thus mixing binary particles in a gasification reactor. For a given gas velocity, the bubbling behavior of the fluidized bed can be characterized by the bubble properties such as bubble diameter, bubble rise velocity, and bubble frequency. The bubbles in dense fluidized beds are the regions where the particle concentration is low, whereas the region with higher solid concertation is referred to as the emulsion phase. As the fluidizing gas passes through the lower part of the bed (from the distributor), bubbles are formed. The bubbles grow in size, merge, split, and may disappear as they move within the bed. The bubble size in the fluidized bed is influenced by the air distribution, particle size distribution, bed geometry, superficial gas velocities, and bed height [7,8]. When the bubble size grows and equals the bed diameter, the bed tends to shift from bubbling to slugging, and the types of slugs can be axial slugs, wall slugs, and flat slugs [5]. There can be a slug in a bed with a smaller reactor diameter even if the bubble size is smaller than the bed diameter. Kunii et al. [5] showed that wall effect retards the rise velocity of the bubble when the ratio between bubble diameter and bed diameter is greater than 0.125 and also illustrated that when the ratio between bubble diameter to bed diameter is greater than 0.6, the bed transits from bubbling to slugging. The large size bubbles in the bed mean increased bubble rise velocity; thus, the bubbles may bypass the bed, reducing the residence time of gas phase and gas-to-solid contact time inside the reactor. Therefore, operating the bubbling bed with optimal bubbles size, velocity, and frequency is crucial for reactor safety and efficient fuel conversation.

Measurement Techniques in a Fluidized Bed

The fundamental understanding of bubble solid hydrodynamics in a fluidized bed can be achieved from the bubble properties that include bubble shape and size, bubble rise velocity, bubble frequency, etc. [8–10]. The bubble properties in a fluidized bed can be measured from experimental measurements and CFD simulations that produce reliable data. Several experimental measurement techniques have been proposed to measure the properties of fluidized bed and study its fluid dynamics behavior [11,12]. The measurement techniques broadly include intrusive techniques and non-intrusive techniques. The intrusive techniques consist of resistance, inductance, and thermal probes [13,14], while the non-intrusive techniques are based on imaging, laser, and tomography methods [15,16]. The major disadvantages of intrusive measurement techniques are that insertion of the probe inside the bed hinders the fluid dynamics behavior. The non-intrusive measurement techniques, on the other hand, can be used to measure bubble properties without interfering the flow hydrodynamics. Among the non-intrusive techniques (X-ray, γ-ray, and Ultrasonic tomography), electrical capacitance tomographic (ECT) is faster and can be used in real-time applications [15]. The ECT measurement techniques employ sensors that measure the relative permittivity between two non-conducting phases. The bubble

properties, for instance, bubble diameter and frequency, can be calculated based on the solid-to-void fraction extracted from the permittivity measurement. The velocity of bubbles can be obtained via a reconstruction method, for example, cross-correlation techniques, that gives a measurement of the bubble rising time from one sensor to another sensor position [17]. In such cases, the placement of the sensor is very important since the bubbles may split or coalesce as they rise from one position to another within the bed, making it difficult to track a single bubble. Reducing the spacing between the sensors can address such an issue; however, to avoid signal interference, the sensors cannot be too close. In this regard, another simple non-intrusive method to study the bubble properties in a fluidized bed, for instance, digital imaging technique, can be a reliable technique. With the digital imaging technique, images of the bed hydrodynamics are captured at different time frames, and the bubble properties are identified from the extracted images [18,19]. This work employs the digital imaging technique and ECT sensors for the measurement of bubble properties in a BFB reactor.

The non-intrusive experimental methods have been widely applied to identify the bubble properties; however, there are many challenges associated with experimental techniques. For instance, the experimental methods are expensive, and often such measurements are only carried out on a pilot-scale plant that produces specific results which may not represent the large-scale reactor conditions. Conducting experiments to observe the hydrodynamics properties of fluidized bed large-scale reactors in such a harsh environment and opaque nature of the reactor is extremely difficult. Moreover, to study the influence of different parameters that primarily influence the fluidized bed hydrodynamics, it is impossible to change the reactor dimensions, sensor positions, and other parameters during experimentation. Such experimental difficulties to identify the fluidized bed hydrodynamics can be overcome using Computational Fluid Dynamics (CFD) simulations. Several studies have been carried out to study fluidized bed hydrodynamics using a CFD model in the past. There are mainly two types of CFD approach used to study flow dynamics of the fluidized bed: the Eulerian-Eulerian method (continuum) and Eulerian–Lagrangian method (Continuum-Discrete) [20,21]. In the Eulerian-Eulerian approach, one particle phase is considered where only two interacting phases exist, one particle phase and the gas phase, which is called as Two-Fluid Model (TFM). TFM is widely used to study and simulate fluidized bed hydrodynamics [22,23]. However, the major drawback with the TFM method is that it accounts for the particles with the same density, diameter, and coefficient of restitution which often results in inaccurate prediction of the bed properties [24]. In the Eulerian–Lagrangian approach, discrete element models (DEM), on the other hand, are more reliable and predict better results than TME [25]. Individual particles are tracked with the DEM method, and particle–particle collision is considered, unlike the TFM model. Therefore, DEM requires enormous computing power to simulate real fluidized bed systems. Another Eulerian–Lagrangian approach, CPFD, that uses a multiphase particle-in-cell approach (MP-PIC), has gained popularity recently due to its capacity to simulate natural fluidized bed systems. In the MP-PIC approach, particles with the same properties, such as density, volume, etc., are grouped to form a parcel. Barracuda V.R. is a commercial CPFD software that uses the MPIC approach to simulate real fluidized bed systems [26,27]. Many studies have focused on using CPFD to study different fluidized bed systems [28,29]. Despite existing studies, there are some publications with the CPFD model on 3D bubbling fluidized beds that can predict the bubble properties [30]. Proper validation of the CPFD model to predict bubble properties of the bubbling fluidized bed with experimental work is still needed. In addition, digital imaging techniques applied for the measurement of the bubble properties from the three-dimensional CPFD simulation with experimental validation are scarce.

This work investigates the fluid dynamic behavior and bubble properties of a BFB reactor with Geldart B particles using CPFD simulations. The fluid dynamic behavior of a BFB was characterized from the bubble properties: bubble diameter, bubble rise velocity, and bubble frequency. The bubble properties were measured from the images

extracted from the plane at transient simulation time step. To illustrate the robustness of the CPFD model, the properties of the bed measured from the CPFD model at each superficial gas velocity are compared with the experimental data and different correlations. The experimental work has been carried out at an ambient condition on a bubbling fluidized bed with ECT sensors. The 2D raw data obtained from the ECT measurements are processed in MATLAB to measure the bubble properties.

2. Materials and Methods

2.1. Computational Particle Fluid Dynamic Model

The simulations in this work were carried out using the CPFD software Barracuda VR, which is commercial software specially designed for the application in multiphase flow systems such as fluidized bed reactors. Unlike other CFD software, the main advantages of using Barracuda VR are that it facilitates defining particle species with particle size distribution. It allows to define and simulate computational particles in order of 10^{15} and higher. Additionally, it uses 3D multiphase particle-in-cell approach for simulation of gas-particle flows and considers fluid-particle coupling with detailed consideration of thermal physics and reaction chemistry. For the fluid-particle simulations, Barracuda virtual reactor uses a combined Eulerian and Lagrangian approach where the solid particles are modeled as discrete Lagrangian methods and the fluid is modeled as Eulerian grid of cells. To create a virtual reactor in any CFD tool, the first step was to set up a grid that defined the control volume, cells, and boundary conditions for all fluid field calculations. A CAD geometry (equal to experimental reactor setup) was drawn in STL format in SolidWorks and imported to Barracuda VR to define grids. A total of 102,400 cells were specified with a uniform grid generation option available in Barracuda that divides the rector into cells uniformly. The number of cells (102,400) was defined so that the cross section of the reactor is divided into 32 × 32 pixels similar to the experimental set up. Three planes were set up at heights of 5 cm, 10 cm, and 15.7 cm along vertical direction of the reactor (Figure 1a). Flow and pressure boundary conditions are defined at the bottom and top of the reactor, respectively (Figure 1a). The solid volume fraction of the bed is set as 0.543 at the static condition, which is obtained experimentally by dividing the bulk density of the bed material with particle density. The parameters used for the development of the simulation model are summarized in Table 1. The details of the mathematical descriptions of the computational model in Barracuda can be found elsewhere [31–34].

Table 1. Simulation parameters used for the model development in a BFB reactor.

| Parameters	Value
Particle density,	2650 kg/m^3
Particle diameter	302.46 μm
Gas density	1.225 kg/m^3
Bed diameter	10.4 cm
Initial bed height	30 cm
Superficial gas velocity	(0.137–0.4) m/s
Close pack volume fraction	0.64
Particle volume fraction	0.534
Total number of cells	102,400
Time step	0.001
Simulation time	60 s
Minimum fluidization velocity, U_{mf}	0.07 m/s
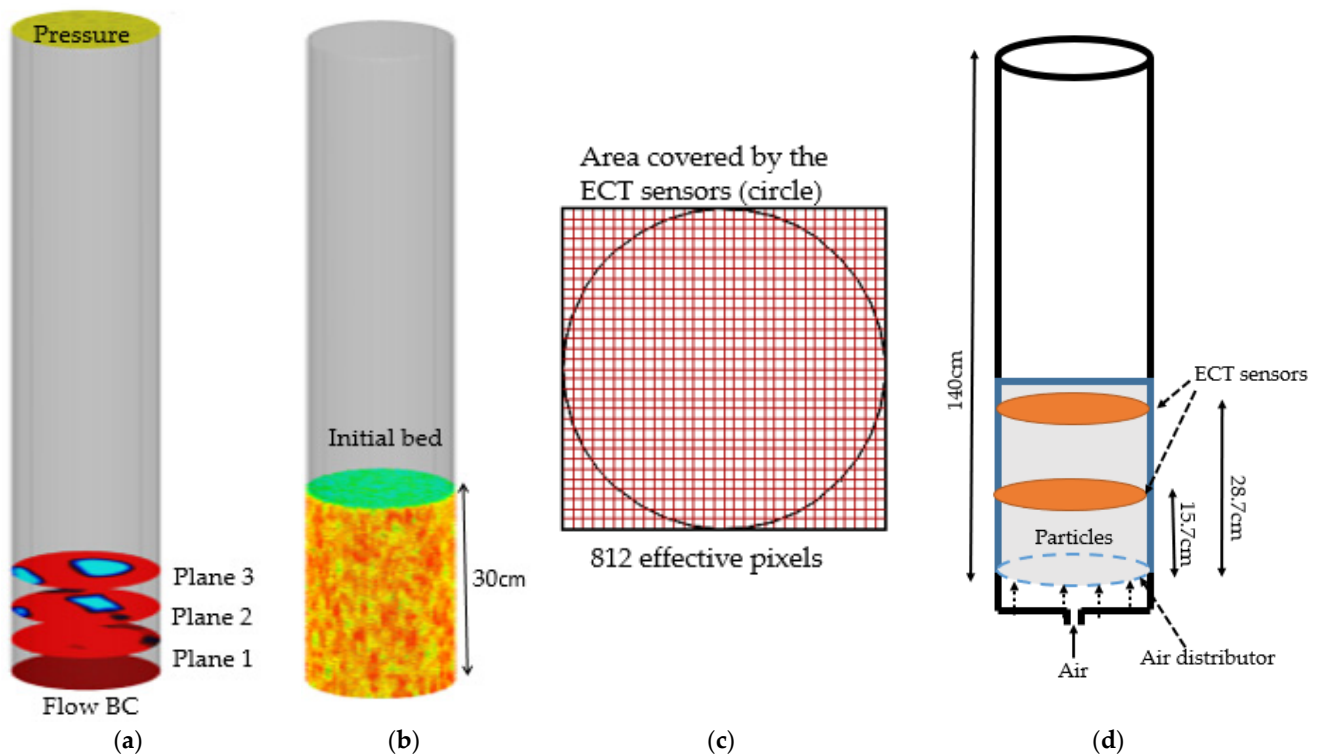
Figure 1. (**a**) Flux planes along the vertical height and boundary conditions; (**b**) initial bed height in CPFD model; (**c**) area covered by the ECT sensors; (**d**) schematic diagram of the experimental setup.

The drag model in a fluidized bed is an important function which determines the force acting on the particles by the fluid flow around it. For the drag force calculation, the combined drag model, Wen-Yu and Ergun, is used with non-linear coefficient 2 and linear coefficient 180 [19]. Several studies showed a better prediction of the bubbling fluidized bed reactor using the blended Wen-Yu and Ergun drag model [1,35]. Similarly, the wall effect has a significant influence on the bubble properties and bed hydrodynamics and is significant in a fluidized bed reactor. In this study, the effect of the wall on the fluid particle motion is considered in terms of normal-to-wall momentum retention, and tangent-to-wall momentum retention. Normal-to-wall momentum retention is defined as the normal component of the particle momentum retained after the particle collision with the wall. When the particle collides with the wall, it tends to lose normal and tangential momentum. The tangential component of the particle momentum retained by the particle after collision with the wall is defined as the tangent-to-wall momentum retention.

Figure 2 illustrates the mathematical implementation of the parameters: tangent-to-wall momentum and normal-to-wall momentum retention, where u^{n+1} is the particle speed after collision and u^n is the particle speed before collision. The values 0.85 and 0.85 are selected for the tangent-to-wall momentum retention and normal-to-wall momentum retention, respectively. The value of 0.85 in normal-to-wall momentum means 85% of the momentum is retained. The sand particle is modeled as a hard sphere, and the values of these parameters are used as suggested in the literature [36]. These losses of the normal and tangential momentum with wall impact are described in Equation (1).

$$u^{n+1} = [(r_T - r_N)(1 - \cos\theta + r_N][u^n] \tag{1}$$

where r_T, and r_N are momentum retention factor for a tangential wall impact and momentum retention factor for a normal wall impact, respectively.
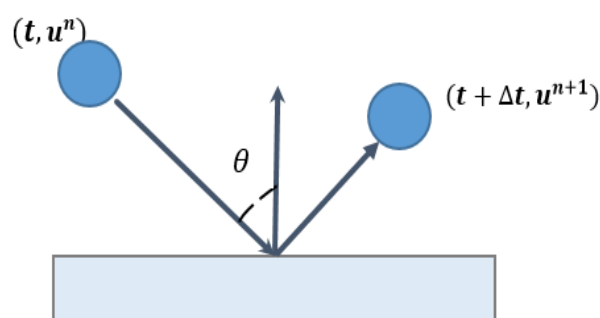
**Figure 2.** Illustration of momentum retention of the particle.

2.2. Experimental Setup

The experimental measurement technique in this work includes the use of electrical capacitance tomography sensors for the measurement of bubble properties in a bubbling fluidized bed reactor. The experimental setup consists of a 10.4 cm internal diameter reactor column equipped with the twin-plane ECT sensors and a data acquisition system. The twin-plane ECT sensors are located at 15.7 cm and 28.7 cm along the reactor height, as shown in Figure 1d. Each ECT sensor is composed of 12 equally spaced electrodes mounted on the outer wall of the reactor. The fluidizing gas is passed uniformly through the particle bed via an air distributor located at the bottom of the reactor. The raw data produced from the ECT sensors are either in the form of a numerical matrix or image that covers the entire sensor-measuring area. The cross-section of each sensor is divided into 32×32 square pixels, of which 812 are the effective pixels that lie within the bed (shown in Figure 1c). Each pixel holds a normalized relative permittivity value between 0 and 1, which represents the gas–solid fraction. The system was calibrated before experiments. The calibration was performed for both the extreme cases, i.e., when the sensor area is filled with higher permittivity material (air) and lower permittivity material (sand particles). Sand particles are used as the bed material and compressed air as the fluidizing gas. The properties of particles used are shown in Table 1. The data sampling frequency is sensitivity to local gas–solid fraction measurements in the fluidized bed. For instance, Yassir et al. [37] demonstrated the sensitivity of measurement span while using ECT sensors and suggested a 60 s measurement span for the extraction of reliable data in a bubbling fluidized bed. In this work, for each flow velocity, the data were logged for 60 s with a time step of 0.01 that produced a total of 6000 frames. Experiments were carried out at different airflow velocities, and the influence on bubble properties (bubble diameter and bubble frequency) was determined. Due to the large distance between the planes in the experimental set up (shown in Figure 1d), it was difficult to track the same bubble for the measurements of bubble rise velocity. As the bubbles rose from a plane at 15.7 cm to another plane at 28.7 cm, as shown in Figure 1d, the bubbles merged into a single large bubble or split into smaller bubbles (due to large distance between the measurement sensors). Therefore, bubble rise velocity was measured from the simulation data by tracking the centroid position in 3D bed, which is discussed in Section 2.3.

2.3. Methodology and Post-Processing the Simulation Data

Post-processing of the three-dimensional simulation data is significant for the analysis of the bed fluid dynamics behavior. In this work, MATLAB and Tecplot were used for data analysis and visualization. Barracuda VR 20.1 comes with a 3D data visualization and data extraction software Tecplot 360 EX (CPFD software Barracuda VR, Houston, TX, USA). The hydrodynamics of the bed was determined by measuring the bubble properties (bubble diameter, bubble rise velocity, and bubble frequency). In order to calculate the bubble properties, the first step was to identify the bubbles at different positions. The bubble position was defined by the region where the solid volume fraction reaches zero. Based on a threshold value of the solid–gas fraction of 0–0.2, the bubbles in the bed were

distinguished from the emulsion phase. In this work, a threshold value of ≤0.2 (solid volume fraction) was used to characterize the bubble region. The solid volume fraction of 0.2 is selected based on the suggestion made in previous studies [10]. To confirm the applicability of such a gas–solid threshold in this study, careful observation of the boundary region was carried out by checking the solid volume fraction of cells in the boundary region between the bubble and emulsion phase (as shown in Figure 3b). The bubble and its properties were determined from the images extracted from 2D horizontal and vertical planes.
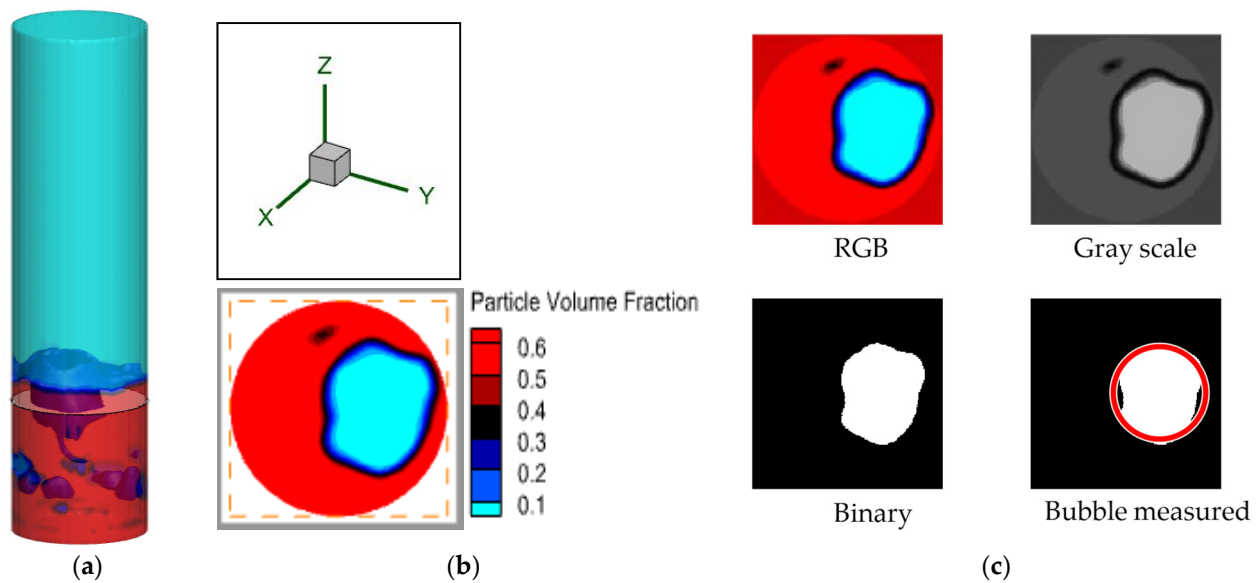
Figure 3. (**a**–**c**) Bubble measured from the extracted images from XY-plane (horizontal plane) at a height of 25.8 cm and superficial gas velocity of 0.25 m/s (The red circle represents equivalent bubble area).

The change in fluidization behavior of the bed with time at different gas velocities was captured in the form of images. For each superficial gas velocity, the simulation time was 60 s, and the images were extracted at 100 frames per second. Therefore, a total of 6000 frames (images) were produced for each selected superficial gas velocity. For the measurement of the bubble properties along the horizontal planes, the images were produced from the post-processing tool Techplot 360 available in Barracuda VR at the pre-defined planes along the vertical height. The extracted images were in RGB format. The images were converted into grayscale images and the grayscale images were further converted into binary images using a MATLAB code. Based on the bubble–solid threshold value (solid volume fraction ≤0.2), the bubble regions were identified from the binary images using the "image processing tool" available in MATLAB. The bubbles were identified as the objects and their properties such as centroid, area, and perimeter were calculated using the regionprops function available in MATLAB. Figure 3a–c shows the method adopted in this work to extract bubbles in the bed along the horizontal plane. The instantaneous three-dimensional iso-volume fraction of the bubbles rising in the bed is shown in Figure 3a. The two-dimensional view of a bubble as it reached plane 3 is illustrated in Figure 3b, and the stepwise method employed to measure the bubble from extracted 2D images is shown in Figure 3c.

Similarly, for the measurement of bubble properties along the vertical planes, the images were extracted at 100 frames per second for each gas velocity. In this case, the bubbles were identified from the RGB to binary images with a bubble ID assigned for each bubble. As the bubbles moved from one position to the upper part of the bed, the bubbles disappeared, split into two or more bubbles, or merged into a single bubble. Therefore, it was important to track the individual bubble to correctly calculate its properties as it

changed from one frame to another. For this reason, a unique bubble ID was assigned for each bubble, as shown in Figure 4. The ID contained information about the bubble name (with the number), bubble height, and diameter, which were used to track the individual bubbles as it moved from one position to another with time. The calculation of the bubble properties—bubble diameter, bubble rise velocity, and frequency—from both approaches are discussed in the results and discussion part.
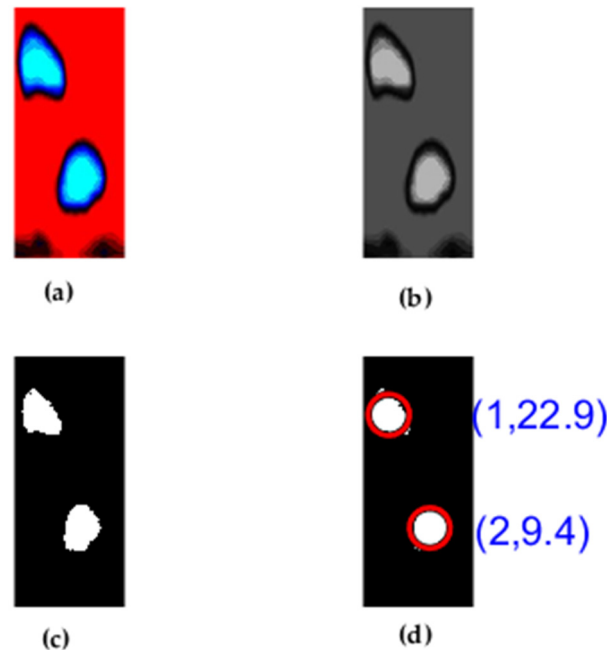
Figure 4. (**a**) RGB image extracted after post-processing; (**b**) grayscale image converted from RGB image; (**c**) binary image converted from grayscale image; (**d**) bubbles (with ID: diameter and position) distinguished from the emulsion phase (The red circle represents equivalent bubble area).

3. Results and Discussion

3.1. Bubble Diameter

The information about average bubble size for a given superficial gas velocity is an important parameter for designing a fluidized bed gasification reactor. In this work, the bubble diameter is determined from the measured bubble area. As a bubble moved vertically and reached the XY plane (plane 3), the area of the bubble was determined. The bubble area was measured by counting (with MATLAB algorithm) the number of pixels occupied by the bubble region. The effective bubble area corresponding to the bed diameter was calculated by multiplying the total effective area of the bed. The average bubble diameter was then calculated by the mean value over the measurement period (60 s).

Figure 5 compares the average bubble diameter obtained from the CPFD simulations, experimental measurement, and correlations for bubble diameter proposed by Mori et al. [38] and Werther et al. [39] (as shown in Equations (2) and (3)). The result depicts that the average bubble diameter increased with an increase in gas velocities. With the increased gas velocity, the bed was diluted with more air, which increased the void fraction. In addition, fluidizing gas in the fluidized bed tends to pass in the form of bubbles, which increased the average bubble size with an increase in superficial gas velocity. However, the increase in bubble diameter as measured from the CPFD simulation was not linear as compared to the correlations proposed by Mori et al. and Werther et al. The CPFD model predicted the average bubble diameter close to the experimental data for the selected superficial gas velocity, while it predicted the average bubble diameter close to Mori et al. correlations up to 0.3 m/s. With a further increase in gas velocity beyond 0.3 m/s, the average bubble diameter increased slightly. At this superficial gas velocity, the average bubble diameter increased up to 0.62 times the bed diameter. There were some bubbles in

the bed that approximately covered the bed diameter, which could convert into slug. With the increase in gas velocity, such bubbles tend to split as they rise in the bed.
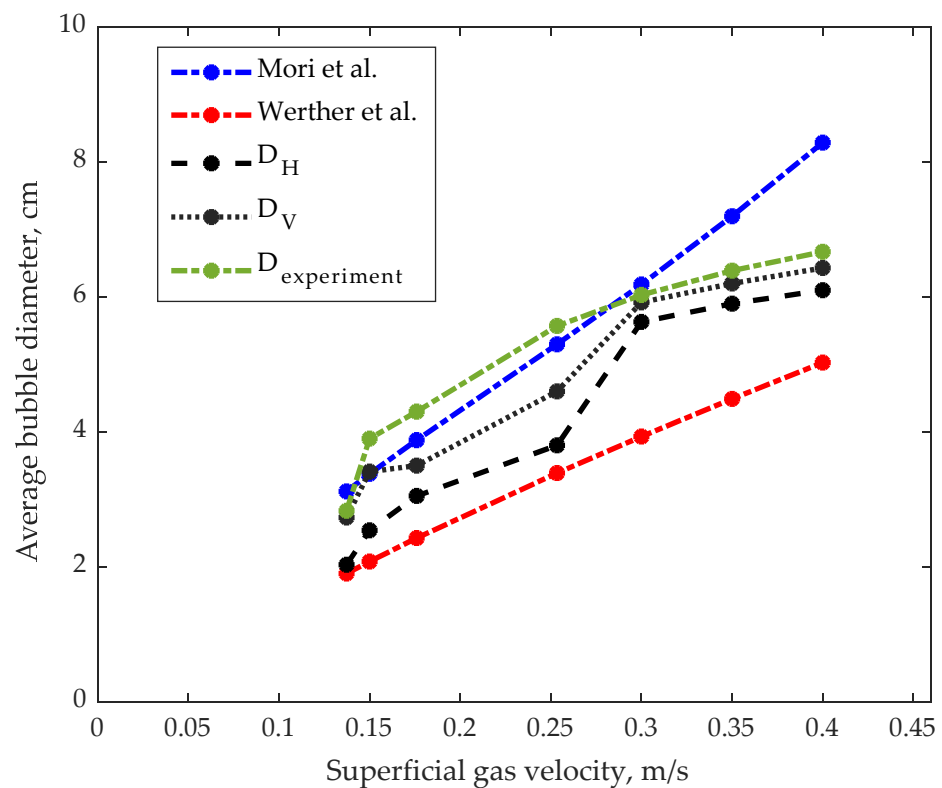
$$d_b = 0.652 \left[A \left(U_0 - U_{mf} \right) \right]^{0.4} - \left(0.652 \left[A \left(U_0 - U_{mf} \right) \right]^{0.4} - d_{b0m} \right) \exp \left(-0.3 \frac{h}{D} \right) \quad (2)$$

$$d_{b0m} = 0.00376 \left(U_0 - U_{mf} \right)^2$$

where d_b, h, D are in [cm] and U_0, U_{mf} are in [cm/s]. A is cross sectional area of the bed, and d_{b0m} is the initial bubble size near the distributor.

$$d_b = d_0 \left[1 + 0.272 \left(U_0 - U_{mf} \right) \right]^{1/3} (1 + 0.0684h)^{1.21} \quad (3)$$

where $d_0 = 0.853$ for Geldart B particles.

Figure 5. Comparing average bubble diameter for different superficial gas velocities obtained from CPFD simulations, experimental data, and different correlations (D_H and D_v are the average bubble diameter measured along the horizontal and vertical planes from the CPFD simulations, respectively) at 15.7 cm along the reactor height [38,39].

Similarly, Figure 6 compares the average bubble diameter from the CPFD model and the correlations at heights of 10 cm and 5 cm for different superficial gas velocities. The results show that the average bubble diameter at both bed heights increases with increasing superficial gas velocity, similar to that of plane 3. However, no slug appeared in the bed up to a height of 10 cm at the selected gas velocities. The average bubble diameter predicted by the CPFD model is in better agreement with the correlation proposed by Mori et al, while the Werther et al. correlation underpredicts the average bubble diameter at height 10 cm. For the bubbles reaching the lower plane at 5 cm, the average bubble diameter measured from the CPFD results agrees well with the Mori et al. correlation for all gas velocities; however, it is only in good agreement with the Werther et al. correlation up to gas velocity 0.25 m/s. The Werther correlation underpredicts the average bubble diameter at superficial

gas velocities higher than 0.25 m/s. The information about the average bubble diameter for the given bed conditions (fluidization velocity, aspect ratio, bed diameter, etc.) are useful for characterizing the bed fluidization quality. For instance, a bubble that is too large in the bed means either the bubble can convert into a slugging bed, or it may bypass the bed. On the other hand, if the bubble size is too small, it may not provide uniform mixing in case of a bed with a binary mixture of particles.
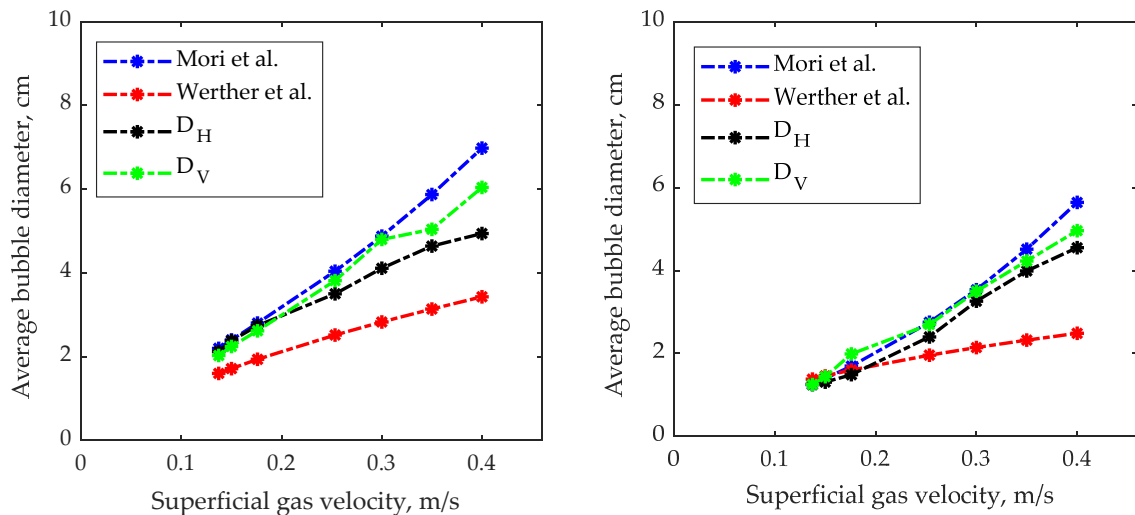
Figure 6. Average bubble diameter for different superficial gas velocities at height 10 cm (left side) and 5 cm (right side) [38,39].

3.2. Bubble Rise Velocity

The bubble rise velocity was estimated by using a detailed signal analysis method and a bubble displacement method. The bubble rise velocity from the detailed signal analysis method was obtained from the fluctuation of solid volume fraction from two planes at heights of 10 cm and 5 cm for each bubble passage. As the bubbles rise from plane 2 to plane 1, there is a time lag (Δt) between each bubble passage, as shown in Figure 7. The bubble rise velocity (U_{b1}) is obtained based on the distance between two planes (ΔH), as shown in Equation (4).

$$U_{b1} = \sum \frac{\Delta H}{\Delta t} \, , \ \Delta t = t2 - t1 \tag{4}$$
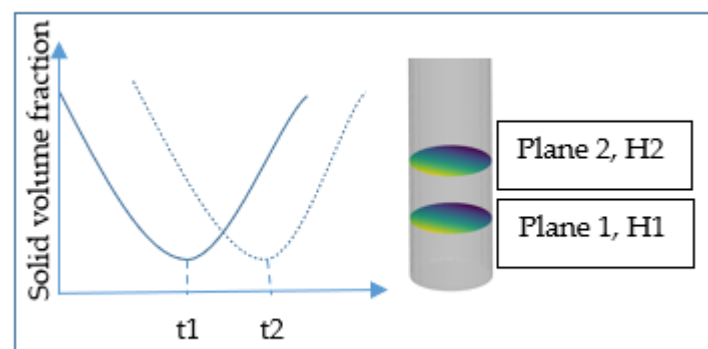
Figure 7. Schematic diagram showing the fluctuation of solid volume fraction as the bubble passes the planes.

When calculating the bubble rise velocity with the bubble displacement method, the bubble is tracked as it passes from one time step to another. As the bubbles move from one position to another, its centroid position changes, and the bubble displacement has

been calculated from the centroid positions in consecutive time steps. The bubble rise velocity, U_{b2}, is calculated from Equation (5).

$$U_{b2} = \sum \frac{\Delta d}{\Delta t} \tag{5}$$

$$\Delta d = \sqrt{(X_2 - X_1)^2 + (Y_2 - Y_1)^2}$$

where Δd is the displacement of the bubble centroid positions. (X_2, Y_1), (Y_1, Y_2) are the centroid positions in the consecutive time frames.

Figure 8a shows the fluctuation of the solid volume fraction from the simulation result at superficial gas velocity 0.25 m/s. As shown in Figure 8b, there is a time lag as the bubble moves from the lower plane to the upper plane. By measuring the time difference, the bubble rise velocity is calculated from the plane positions. The average bubble rise velocity as the bubble reaches 15.7 cm bed height at different superficial gas velocities is shown in Figure 9d. The experimental measurement of the bubble rise velocity was not possible, and therefore, the bubble rise velocity obtained from the CPFD model is compared with correlations for bubble rise velocity from the literature. The correlations proposed by Davidson et al. [40] and Agu et al. [41] have been used for the comparison. The result shows that the average bubble rise velocity increases with an increase in superficial gas velocity. With an increase in superficial gas velocity, the bubble diameter increased which increased the rise velocity of the bubbles in the bed. The bubble rise velocity predicted by the CPFD model does not increase linearly at different gas velocities, as predicted by the correlations. However, the bubble rise velocities predicted by the CPFD model are in agreement with the correlations. The CPFD model predicts the bubble rise velocity at different superficial gas velocities closer to the correlation proposed by Agu et al., while the correlation proposed by Davidson et al. overpredicts the bubble rise velocity. This is because the correlation proposed by Agu et al. is an improved version of the Davidson et al. correlation, where the author has proposed a correlation for bubble velocity based on the bubble-projected area.
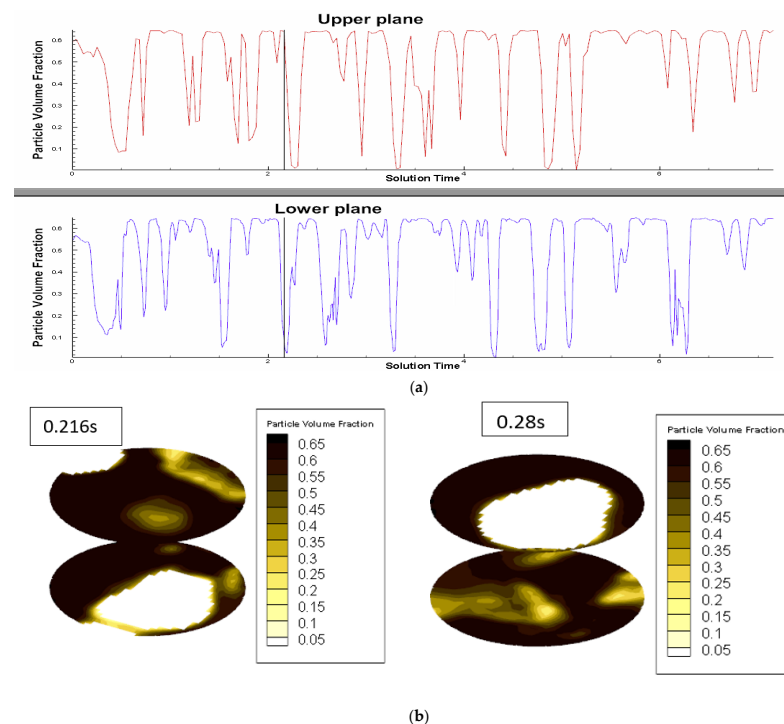
Figure 8. (**a**) Fluctuation of solid volume fraction as the bubble passes from lower plane to upper plane. (**b**) Mapping of the bubble on the lower plane and upper plane at different time steps.
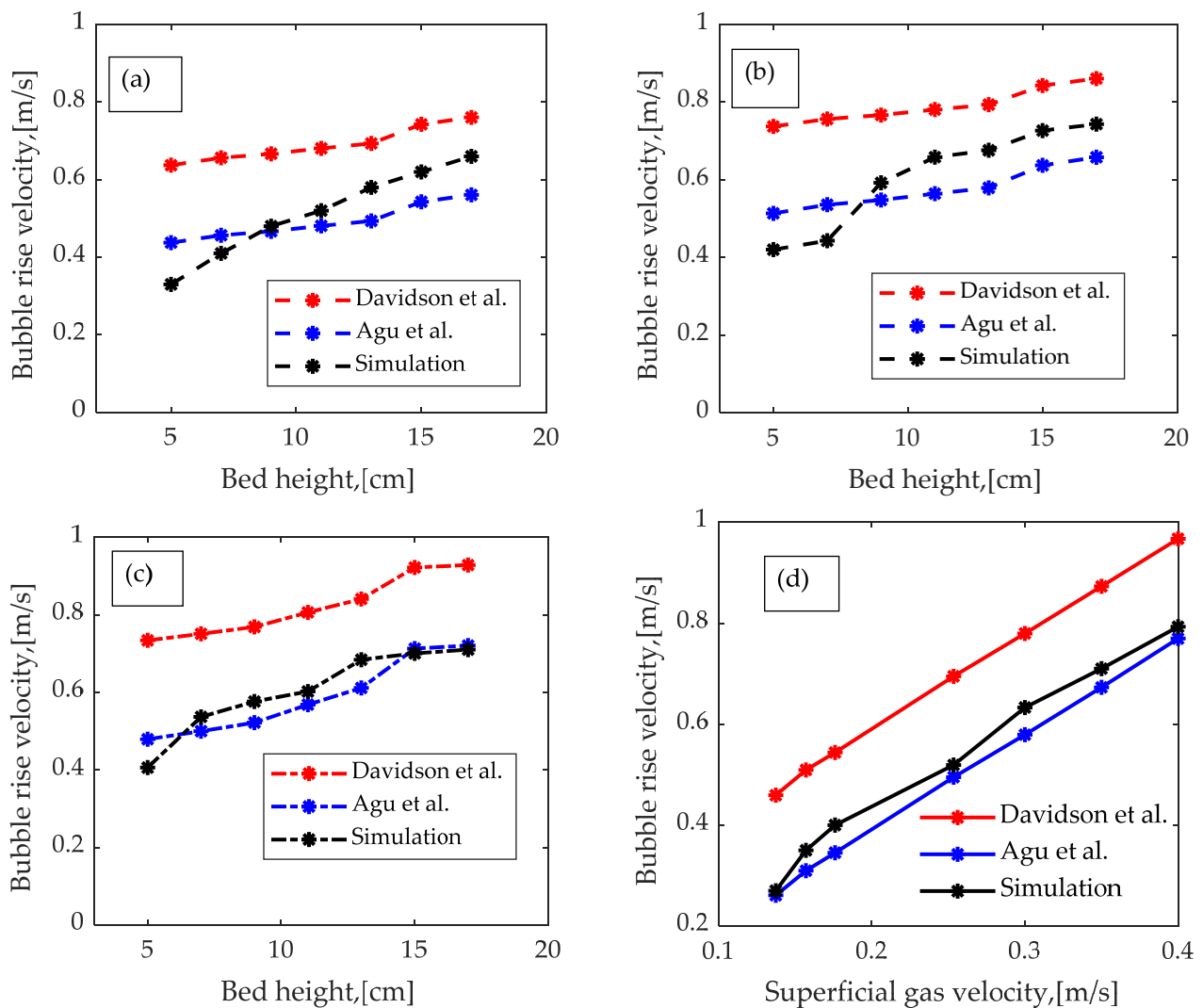
Figure 9. (**a**–**c**) Bubble rise velocity vs. bed height at different gas velocities of 0.13 m/s, 0.35 m/s, and 0.4 m/s, respectively; (**d**) average bubble rise velocity as the bubbles moved from the plane at 10 cm to the plane at 15.7 cm at different superficial fluidizing gas velocities [40,41].

With the above method, tracking a bubble and measuring its rise velocity at the predefined plane, the chances are that the bubble may disappear, split, or coalesce, making it difficult to track its properties. Therefore, tracking the bubble rise velocity from one frame to another is more reliable as it does not lose any information. In order to calculate the rise velocity of the bubble as it moves, the easiest way is to measure the rise velocity by tracking the centroid position with time as discussed earlier. Figure 9a–c shows the mean bubble rise velocity at different superficial gas velocities and positions along the reactor height. The bubble rise velocity is obtained from the centroid positions (Equation (5)) as it moves from one frame to another. The result shows that the bubble rise velocity increases with an increase in superficial gas velocity 0.137 m/s to 0.4 m/s. Additionally, the bubble rise velocity increases as the bubble moves from the lower region to the upper part of the bed. Comparing the calculated bubble rise velocity from the CPFD model with the correlations of bubble rise velocity, the results illustrate that the CPFD model underpredicts the bubble rise velocity at the lower positions of the bed. At the upper part of the bed, the bubble rise velocity is higher than predicted by Agu et al. but lower than the Davidson et al. correlations. At the gas velocity of 0.137 m/s, the bubble rise velocity increases gradually with height, indicating that small bubbles are formed at the lower part of the bed. The bubble size and rise velocity increase gradually as the bubble moves from the lower

section to the upper section (as shown in Figure 9a). At superficial gas velocity of 0.35 m/s (Figure 9b), the bubble rise velocity increases slowly below 10 cm bed height, and there is a sudden increment in the bubble rise velocity afterward; this is due to coalescing of the smaller bubbles into large bubbles, which increases the rise velocity of the bubble.
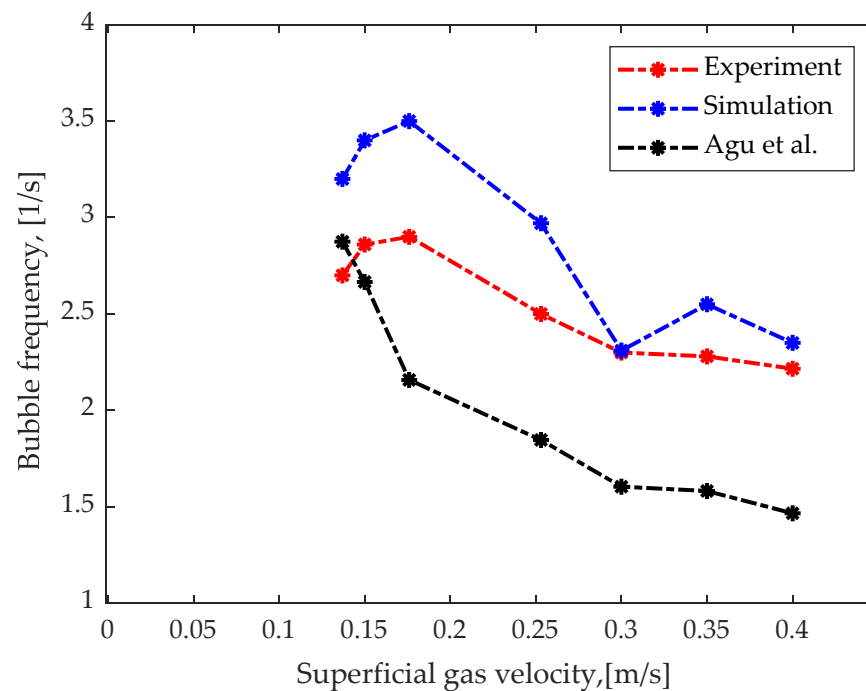
3.3. Bubble Frequency

The bubble frequency is an important parameter influencing the gas and solid residence time inside the bubbling fluidized bed. There are many approaches to calculating the bubble frequency inside the bed. The simplest method is to count the number of bubbles over the measurement period [42]. Another approach is to plot the power spectrum density to obtain the bubble frequency [43]. In this work, the bubble frequency is obtained using both methods. The bubbles passing through a plane along the vertical height are measured, and the bubble frequency is calculated from Equation (6). Figure 10 shows the histogram plot of the number of bubbles of varying diameters counted at each superficial gas velocity over the measurement time. As can be seen from the figure, bubbles of different sizes pass the plane at height 15.7 cm. However, up to the superficial gas velocity of 0.25 m/s, there are many bubbles with smaller diameters. Therefore, operating the fluidized bed regimes below 0.25 m/s for this case can be effective, provided that the particles (in the case of bed with binary particles) do not segregate.

$$Bubble\ frequency,\ f_b = \frac{Total\ number\ of\ bubbles\ passing\ the\ plane}{sampling\ time} \tag{6}$$
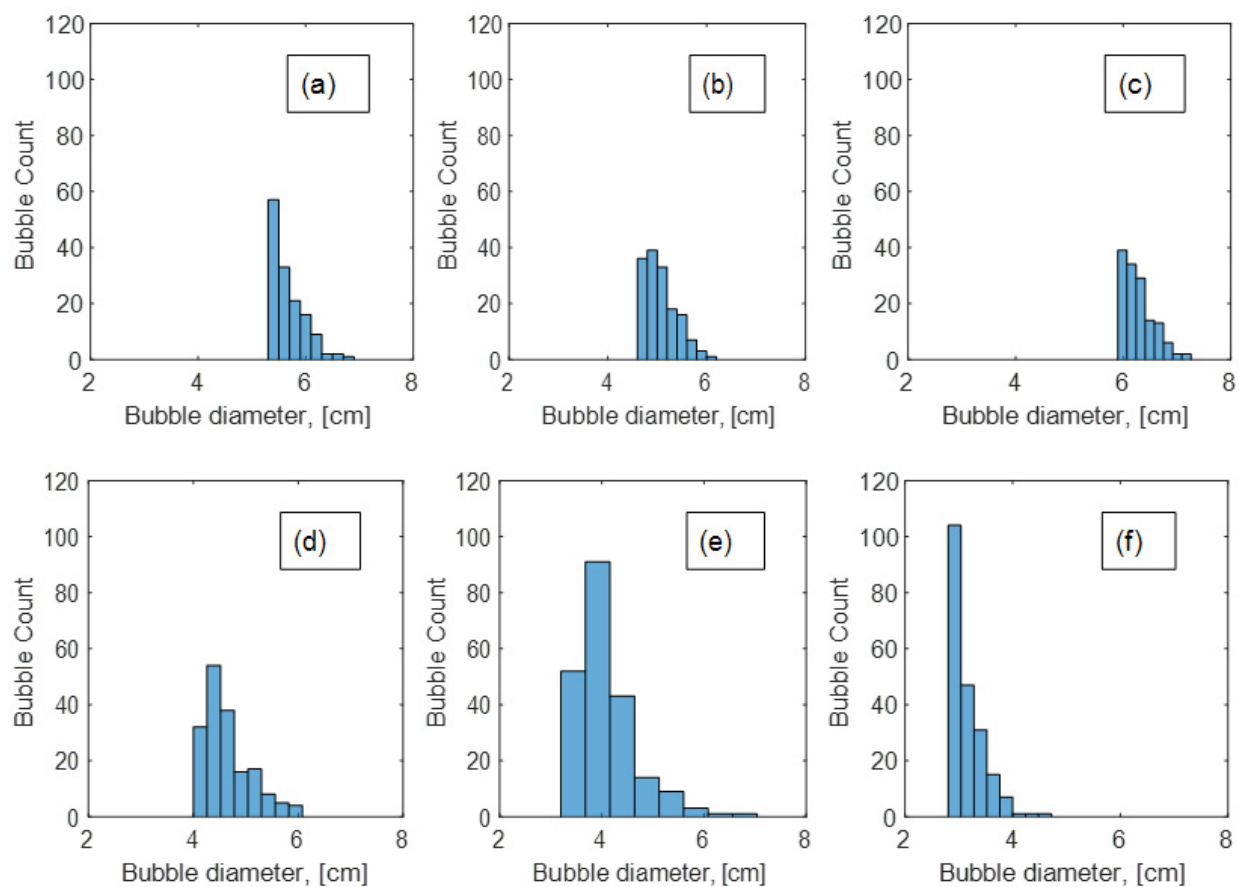
Figure 10. Bubble count vs. bubble diameter at superficial gas velocities of 0.4 m/s, 0.35 m/s, 0.3 m/s, 0.25 m/s, 0.176 m/s, and 0.15 m/s illustrated in the pictures from (**a–f**), respectively.

The plot of bubble frequency at different superficial gas velocities from the CPFD model, ECT measurement, and Agu et al. [41] correlation are compared in Figure 11. The result from the CPFD model shows that bubble frequency increases with an increase in superficial gas velocity up to 0.25 m/s and decreases further. The increase in bubble frequency up to 0.25 m/s is due to the formation of a large number of smaller size bubbles in the bed (as shown in Figure 10d–f). Due to the coalescence of the smaller bubbles to form larger diameter bubbles, the bubble frequency decreases for the higher gas velocities. At superficial gas velocity of 0.35 m/s, there is a slight increment in the bubble frequency due to split of the large diameter bubbles. The CPFD model predicts the bubble frequency close to the experimental data at higher gas velocities and overpredicts the bubble frequency at lower gas velocities. However, the simulations follow a similar trend of the bubble frequency as the experimental measurements. The Agu et al. correlation for the bubble frequency predicts the bubble frequency close to experimental data at lower gas velocities; however, it underpredicts the bubble frequency at higher gas velocities compared to the experimental and CPFD model. This is because the correlation proposed by Agu et al. is developed for deep beds.

Figure 11. Bubble frequency vs. superficial gas velocities at 15.7 cm bed height [41].

The bubble frequency can be obtained from the fluctuation of the solid volume fraction signal. The solid volume fraction fluctuation for each time step is recorded at different gas velocities. An illustration of the fluctuation of the solid volume fraction at superficial gas velocity of 0.4 m/s is shown in Figure 12a. The bubble frequency is obtained from the Fourier transform of the time series plot of solid volume fraction. The Fourier transform of the solid volume fraction at superficial gas velocity of 0.137 m/s, 0.25 m/s, and 0.4 m/s at 15.7 cm bed height is shown in Figures 12b, 12c and 12d, respectively. The amplitude of the solid volume fluctuation is shown on the Y-axis and frequency on the X-axis. The amplitude gives information about the bubble size. For the bed with a single bubble, the frequency can be obtained, where the amplitude is at the maximum. However, for a bubbling fluidized bed, it is evident that there can be multiple peaks for multiple bubbles passing a plane, as shown in Figure 12c,d. The multiple peaks of the varying amplitude depict that there are multiple bubbles with different sizes passing the plane. With an increase in superficial gas velocity from 0.137 m/s to 0.4 m/s, the amplitude increases. This increase in the amplitude is due to an increase in the bubble size. There is no dominant frequency; however, for

each gas velocity, there are several peaks within the band of 1–6 Hz. For gas velocity of 0.137 m/s, the peak of the amplitude fluctuates within a narrow height, which indicates that there are multiple smaller bubbles. At 0.25 m/s, few large bubbles are observed (as indicated by the sudden increase in the amplitude). At superficial gas velocity of 0.4 m/s, the amplitude of the solid volume fraction fluctuation is approximately 60–100 within the band of 2–5 Hz. The higher amplitude with a wide range of bands indicates that the large number of bigger-sized bubbles pass the plane at 15.7 cm.

(a)

(b)

(c)

(d)
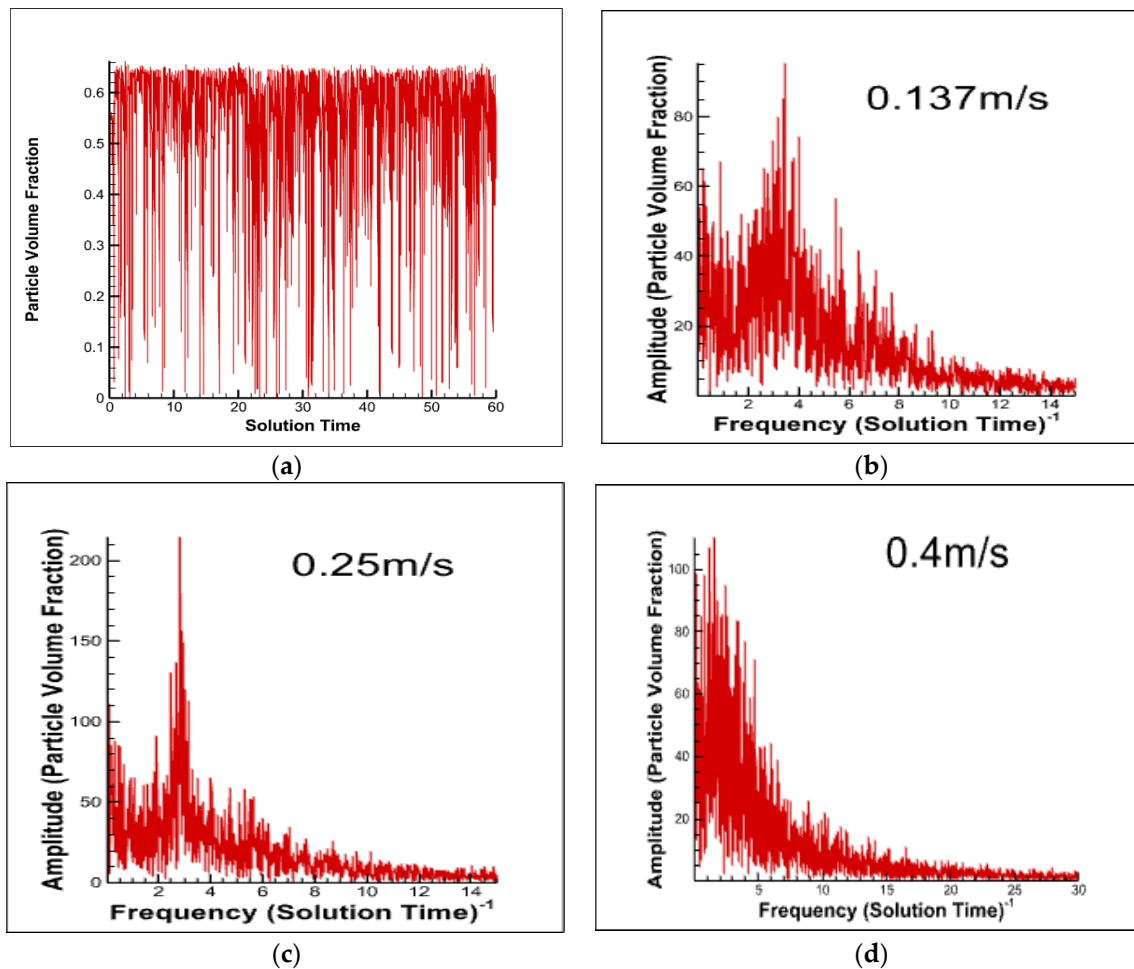
Figure 12. Figure showing: (**a**) fluctuation of particle volume fraction with time; (**b–d**) Fourier transform of the particle volume fraction for superficial gas velocities 0.137 m/s, 0.25 m/s, and 0.4 m/s, respectively.

4. Conclusions

The efficiency of a fluidized bed reactor depends on the bed fluid dynamic behavior, which is significantly influenced by the bubble properties. The bubble properties in a BFB are primarily responsible for heat and mass transfer, better mixing, and solid circulation. This work investigates the bubble properties of a bubbling fluidized bed reactor using computational particle fluid dynamic (CPFD) simulations and electrical capacitance tomography (ECT) measurements. The bubble properties measured in this work include average bubble diameter, bubble rise velocity, and bubble frequency at different superficial gas velocities and heights along the reactor. The two-dimensional images along the reactor horizontal and vertical planes of the BFB were extracted from the CPFD simulations at transient time steps and different operating conditions. The CPFD model was developed in a commercial CPFD software Barracuda Virtual Reactor 20.0.1. The bubble behavior and bed fluidization behavior are characterized from the bubble properties. The bubble

properties were determined by processing the extracted images with script developed in MATLAB. The CPFD simulation results are compared with experimental data from the ECT sensors and correlations in the literature.

The results from the CPFD model and experimental measurement depicted that the average bubble diameter increased with an increase in superficial gas velocities up to 4.2 U_{mf} and decreased with a further increase in gas velocities due to the onset of large bubbles (potential slugging regime). The result predicted by the CPFD model revealed that the bubble rise velocity was directly related to bubble diameter. The rise velocity of the bubbles increased with an increase in superficial gas velocity and bubble position in the bed. However, the increment in bubble rise velocity was not linear. The bubble moved slowly within the lower region of the bed. The bubble velocity increased significantly in the middle and upper region of the bed, followed by bubble coalescence at superficial gas velocity $5U_{mf}$. The Fourier transform of the transient solid volume fraction illustrated that multiple bubbles pass the plane with varying amplitude and frequency in the range of 1–6 Hz. Further, the bubble frequency increases with an increase in superficial gas velocity up to $2.5U_{mf}$ and decreased with a further increase in gas velocity.

The CPFD model and method employed in this work can be useful for the efficient design and operation of a bubbling fluidized bed gasification reactor. Further work will be focused on investigating the influence of bubble properties on gasifier conversion efficiency operated at high temperatures.

References

1. Jaiswal, R.; Agu, C.E.; Thapa, R.K.; Moldestad, B.M.E. Study of fluidized bed regimes using Computational Particle Fluid Dynamics. *Linköping Electron. Conf. Proc.* **2018**, *153*, 271–276. [CrossRef]
2. Jaiswal, R.; Furuvik, N.C.I.S.; Thapa, R.K.; Moldestad, B.M.E. Method of identifying an operating regime in a bubbling fluidized bed gasification reactor. *Int. J. Energy Prod. Manag.* **2020**, *5*, 24–34. [CrossRef]
3. Yang, W.-C. Other nonconventional fluidized beds. In *Handbook of Fluidizfition and Fluid-Particle Systems*; Siemens Westinghouse Power Corporation: Pittsburgh, PA, USA, 2003.
4. Geldart, D.; Baeyens, J. The design of distributors for gas-fluidized beds. *Powder Technol.* **1985**, *42*, 67–78. [CrossRef]
5. Kunii, D.; Levenspiel, O. *Fluidization Engineering*; Butterworth-Heinemann: Oxford, UK, 1991.
6. Johnsson, F.; Zijerveld, R.; Schouten, J.; Bleek, C.V.D.; Leckner, B. Characterization of fluidization regimes by time-series analysis of pressure fluctuations. *Int. J. Multiph. Flow* **2000**, *26*, 663–715. [CrossRef]
7. Issangya, A.S.; Cocco, R.A.; Karri, S.R.; Knowlton, T.M.; Chew, J.W. Bed density and bubble void fraction variation in a fluidized bed stripper. *Chem. Eng. Sci.* **2022**, *260*, 117837. [CrossRef]
8. Agu, C.E.; Tokheim, L.-A.; Eikeland, M.; Moldestad, B.M. Determination of onset of bubbling and slugging in a fluidized bed using a dual-plane electrical capacitance tomography system. *Chem. Eng. J.* **2017**, *328*, 997–1008. [CrossRef]
9. CHOI, J.H.; Son, J.E.; Kim, S.D. Bubble size and frequency in gas fluidized beds. *J. Chem. Eng. Jpn.* **1988**, *21*, 171–178. [CrossRef]
10. Karimipour, S.; Pugsley, T. A critical evaluation of literature correlations for predicting bubble size and velocity in gas–solid fluidized beds. *Powder Technol.* **2011**, *205*, 1–14. [CrossRef]
11. Yang, W.-C. Bubbling fluidized beds. In *Chemical Industries-New York-Marcel Dekker-*; Siemens Westinghouse Power Corporation: Pittsburgh, PA, USA, 2003; pp. 53–112.
12. Glicksman, L.; Lord, W.; Sakagami, M. Bubble properties in large-particle fluidized beds. *Chem. Eng. Sci.* **1987**, *42*, 479–491. [CrossRef]

13. Liu, J.; Grace, J.R.; Bi, X. Novel multifunctional optical-fiber probe: I. Development and validation. *AIChE J.* **2003**, *49*, 1405–1420. [CrossRef]

14. Du, B. *Hydrodynamics and Flow Structure, Gas and Solids Mixing Behavior, and Choking Phenomena in Gas-Solid Fluidization*; The Ohio State University: Columbus, OH, USA, 2005.

15. Du, B.; Warsito, W.; Fan, L.-S. ECT studies of gas− solid fluidized beds of different diameters. *Ind. Eng. Chem. Res.* **2005**, *44*, 5020–5030. Available online: https://pubs.acs.org/doi/10.1021/ie049025n (accessed on 31 August 2022). [CrossRef]

16. Sun, J.; Yan, Y. Non-intrusive measurement and hydrodynamics characterization of gas–solid fluidized beds: A review. *Meas. Sci. Technol.* **2016**, *27*, 112001. Available online: https://iopscience.iop.org/article/10.1088/0957-0233/27/11/112001 (accessed on 31 August 2022). [CrossRef]

17. Deen, N.G.; Godlieb, W.; Gorter, S.; Kuipers, J.A.M. An electrical capacitance tomography study of pressurized fluidized beds. In Proceedings of the 13th International Conference on Fluidization-New Paradigm in Fluidization Engineering, Gyeong-ju, Korea, 16–21 May 2010; Available online: https://dc.engconfintl.org/fluidization_xiii/26/ (accessed on 31 August 2022).

18. Caicedo, G.R.; Marqués, J.J.; Ruíz, M.G.; Soler, J.G. A study on the behaviour of bubbles of a 2D gas–solid fluidized bed using digital image analysis. *Chem. Eng. Process. Process Intensif.* **2003**, *42*, 9–14. [CrossRef]

19. Li, J.; Agarwal, R.K.; Zhou, L.; Yang, B. Investigation of a bubbling fluidized bed methanation reactor by using CFD-DEM and approximate image processing method. *Chem. Eng. Sci.* **2019**, *207*, 1107–1120. [CrossRef]

20. Lettieri, P.; Mazzei, L. Challenges and issues on the CFD modeling of fluidized beds: A review. *J. Comput. Multiph. Flows* **2009**, *1*, 83–131. [CrossRef]

21. Gidaspow, D. *Multiphase Flow and Fluidization: Continuum and Kinetic Theory Descriptions*; Academic Press: Cambridge, MA, USA, 1994.

22. Wang, W.; Lu, B.; Zhang, N.; Shi, Z.; Li, J. A review of multiscale CFD for gas–solid CFB modeling. *Int. J. Multiph. Flow* **2010**, *36*, 109–118. [CrossRef]

23. Singh, B.K.; Roy, S.; Buwa, V.V. Bubbling/slugging flow behavior in a cylindrical fluidized bed: ECT measurements and two-fluid simulations. *Chem. Eng. J.* **2020**, *383*, 123120. [CrossRef]

24. Acosta-Iborra, A.; Sobrino, C.; Hernández-Jiménez, F.; de Vega, M. Experimental and computational study on the bubble behavior in a 3-D fluidized bed. *Chem. Eng. Sci.* **2011**, *66*, 3499–3512. [CrossRef]

25. Wang, J.; van der Hoef, M.A.; Kuipers, J. Comparison of Two-Fluid and Discrete Particle Modeling of Dense Gas-Particle Flows in Gas-Fluidized Beds. *Chem. Ing. Tech.* **2013**, *85*, 290–298. [CrossRef]

26. Kraft, S.; Kirnbauer, F.; Hofbauer, H. CPFD simulations of an industrial-sized dual fluidized bed steam gasification system of biomass with 8 MW fuel input. *Appl. Energy* **2017**, *190*, 408–420. [CrossRef]

27. Cha, B.; Kim, J.; Son, S.R.; Park, D.S.; Il, M. CPFD simulation of fluidized bed flow in FCC regenerator. In *Computer Aided Chemical Engineering*; Elsevier: Amsterdam, The Netherlands, 2012; pp. 1153–1157. [CrossRef]

28. Thapa, R.K.; Frohner, A.; Tondl, G.; Pfeifer, C.; Halvorsen, B. Circulating fluidized bed combustion reactor: Computational Particle Fluid Dynamic model validation and gasfeed position optimization. *Comput. Chem. Eng.* **2016**, *92*, 180–188. [CrossRef]

29. Adkins, B.D.; Kapur, N.; Dudley, T.; Webb, S.; Blaser, P. Experimental validation of CFD hydrodynamic models for catalytic fast pyrolysis. *Powder Technol.* **2017**, *316*, 725–739. [CrossRef]

30. Córcoles, J.; Acosta-Iborra, A.; Almendros-Ibáñez, J.; Sobrino, C. Numerical simulation of a 3-D gas-solid fluidized bed: Comparison of TFM and CPFD numerical approaches and experimental validation. *Adv. Powder Technol.* **2021**, *32*, 3689–3705. [CrossRef]

31. O'Rourke, P.J.; Snider, D.M. Inclusion of collisional return-to-isotropy in the MP-PIC method. *Chem. Eng. Sci.* **2012**, *80*, 39–54. [CrossRef]

32. Snider, D.M. Three fundamental granular flow experiments and CPFD predictions. *Powder Technol.* **2007**, *176*, 36–46. [CrossRef]

33. Snider, D.M. An incompressible three-dimensional multiphase particle-in-cell model for dense particle flows. *J. Comput. Phys.* **2001**, *170*, 523–549. [CrossRef]

34. Andrews, M.J.; O'Rourke, P.J. The multiphase particle-in-cell (MP-PIC) method for dense particulate flows. *Int. J. Multiph. Flow* **1996**, *22*, 379–402. [CrossRef]

35. Weber, J.M.; Layfield, K.J.; Van Essendelft, D.T.; Mei, J.S. Fluid bed characterization using Electrical Capacitance Volume Tomography (ECVT), compared to CPFD Software's Barracuda. *Powder Technol.* **2013**, *250*, 138–146. [CrossRef]

36. Sommerfeld, M.; Huber, N. Experimental analysis and modelling of particle-wall collisions. *Int. J. Multiph. Flow* **1999**, *25*, 1457–1489. [CrossRef]

37. Makkawi, Y.T.; Wright, P.C. Electrical capacitance tomography for conventional fluidized bed measurements—Remarks on the measuring technique. *Powder Technol.* **2004**, *148*, 142–157. [CrossRef]

38. Mori, S.; Wen, C. Estimation of bubble diameter in gaseous fluidized beds. *AIChE J.* **1975**, *21*, 109–115. [CrossRef]

39. Werther, J. Effect of gas distributor on hydrodynamics of gas fluidized beds. *Ger. Chem. Eng.* **1978**, *1*, 166–174.

40. Davidson, J. Fluidized Particles. In *Mobile Particulate Systems*; Springer: Berlin/Heidelberg, Germany, 1995; pp. 173–196.

41. Agu, C.E.; Tokheim, L.-A.; Eikeland, M.; Moldestad, B.M. Improved models for predicting bubble velocity, bubble frequency and bed expansion in a bubbling fluidized bed. *Chem. Eng. Res. Des.* **2019**, *141*, 361–371. [CrossRef]

42. Weber, J.M.; Mei, J.S. Bubbling fluidized bed characterization using Electrical Capacitance Volume Tomography (ECVT). *Powder Technol.* **2013**, *242*, 40–50. [CrossRef]
43. Makkawi, Y.T.; Wright, P.C. Optimization of experiment span and data acquisition rate for reliable electrical capacitance tomography measurement in fluidization studies a case study. *Meas. Sci. Technol.* **2002**, *13*, 1831–1841. Available online: https://iopscience.iop.org/article/10.1088/0957-0233/13/12/305/meta (accessed on 31 August 2022). [CrossRef]